SURVEY OF TYPE I ELM DYNAMICS MEASUREMENTS

by
A.W. LEONARD, L.D. HORTON, Y. KAMADA, A. KIRK, N. OYAMA,
G. SAIBENE, and M.R. WADE

AUGUST 2005

GENERAL ATOMICS

DISCLAIMER

GA–A25161

SURVEY OF TYPE I
ELM DYNAMICS MEASUREMENTS

by

A.W. LEONARD, L.D. HORTON,* Y. KAMADA,[†] A. KIRK,[‡] N. OYAMA,[†]
[£]G. SAIBENE, and M.R. WADE

*Max-Planck-Institut für Plasmaphysik, EURATOM Association, Garching, Germany.
[†]Naka Fusion Research Establishment, Japan Atomic Energy Research Institute, Ibaraki, Japan.
[‡]Euratom/UKAEA Fusion Association Culham Science Center, Abingdon, United Kingdom.
[£]CEA Cadarache EURATOM Association, Cadarache, France.

GENERAL ATOMICS PROJECT 30200
AUGUST 2005

GENERAL ATOMICS

ABSTRACT

This report summarizes Type I edge localized mode (ELM) dynamics measurements from a number of tokamaks, including ASDEX-Upgrade, DIII-D, JET, JT-60U and MAST, with the goal of providing guidance and insight for the development of ELM simulation and modeling. Several transport mechanisms are conjectured to be responsible for ELM transport, including: convective transport due to filamentary structures ejected from the pedestal, parallel transport due to edge ergodization or magnetic reconnection and turbulent transport driven by the high edge gradients when the radial electric field shear is suppressed. The experimental observations are assessed for their validation, or conflict, with these ELM transport conjectures.

I. INTRODUCTION

The rapid release of pedestal energy due to edge-localized-modes (ELMs) has the potential to significantly reduce the lifetime of plasma facing components or could impose severe operational constraints on the divertor operation of next generation tokamaks such as ITER [1]. In order to accurately predict ELM heat flux characteristics for hardware design and to develop mitigation techniques for future tokamaks, it is critical to develop an ELM transport model with predictive capability. This paper summarizes Type I ELM dynamics measurements from a number of tokamaks, including ASDEX-Upgrade, DIII-D, JET, JT-60U and MAST, with the goal of providing guidance and validation for the development of ELM simulation and modeling.

The peeling-ballooning instability, driven by pedestal gradients in both pressure and current has successfully described the experimentally observed edge pressure limit in tokamaks [2]. For tokamaks with Type I ELMs this model typically predicts an instability onset with intermediate toroidal mode number, n = 3-40, with an eigenmode localized to the pedestal steep gradient region. Several observations of Type I ELM precursors are consistent with predictions of this model for characteristics of the ELM onset. In JT-60U and ASDEX-Upgrade Type I precursors have been seen narrowly localized to the pedestal in density from reflectometry and electron temperature from electron cyclotron emission (ECE) [3-6]. These oscillations are at a frequency of 5-25 kHz and start 200-500 µs before an ELM. ELM precursors have also been measured by magnetics probes in DIII-D and JET [7–9] Additionally, the toroidal mode number of the precursors, determined from the magnetic oscillations, has been observed in the range of n = 1-13, generally increasing with density and collisionality. This scaling is in agreement with predictions from the peeling-ballooning model where additional edge bootstrap current at low collisionality stabilizes the instabilities at higher toroidal mode number.

The challenge in modeling and predicting ELM characteristics is in moving beyond a linear description of the ELM instability at its onset to its nonlinear evolution and resulting transport. Initial efforts to simulate the nonlinear evolution of a Type I ELM and resulting transport are now underway [10,11]. In addition, a significant number of tokamak diagnostics are now capable of fast measurements to follow the evolution of the pedestal and scrape off layer (SOL) parameters, and even entire profiles, during an ELM. In this paper various aspects of ELM evolution will be summarized, with an emphasis on implications for ELM transport. Section II summarizes perturbations to the pedestal profiles, and their time dependence, due to the ELM instability. In particular the change in perturbation versus density and collisionality is described. Section III describes SOL and divertor observations that may provide insight into ELM transport. Finally Section IV discusses implications of these observations for the underlying ELM transport mechanisms.

II. PEDESTAL ELM LOSSES

The energy released by a Type I ELM is usually compared across devices and configurations by normalizing the ELM energy by the bulk plasma energy that is potentially accessible to expulsion by ELMs [12]. Normalization by the pedestal energy, as characterized by the total pressure at the pedestal top, ions plus electrons, times the plasma volume has been successful in comparing ELM energy across different plasma configurations and devices of significantly different size. This normalized Type I ELM energy has been observed in a number of tokamaks to vary from more than 20% of the pedestal energy at low density and collisionality to as little as 2%-3% at high collisionality [13]. However, this collisionality relationship can be broken as exhibited by JT-60U and ASDEX-Upgrade where small Type I ELMs, <5% of the pedestal energy, can occur even at low collisionality [14,15]. Understanding and predicting the plasma parameters and other factors that lead to smaller ELM size is especially critical in that an ELM of greater than 10% of the ITER pedestal energy is expected to result in excessive ablation or melting of divertor components [1].

An important aspect of the ELM energy is its variability. A study on JET revealed that the standard deviation in ELM energy is typically 15% of the mean ELM energy [13]. ELM variability is likely a consequence of the highly nonlinear nature of the ELM instability and its evolution. The variability of ELM energy is an important characteristic because ablation of the target is a threshold process dependent on the largest ELMs. Predicting this variability should then be an eventual goal of an accurate ELM model.

The energy transported from the pedestal by an ELM can be examined in terms of its convective losses of electron and ion density and its conductive losses of electron and ion temperature. The reduction of ELM size at higher collisionality was found on DIII-D and JET, to result from a decrease in the temperature perturbation, or conducted energy, while the density loss, or convected energy remained nearly constant [16,17]. This trend is shown in figure 1(a) and (b) for two plasma configurations in JET. The total convected energy lost at an ELM is typically in the range of 5%-10% of the pedestal total. The convected fraction usually remains constant as density and collisionality are varied in any given machine and configuration. Across machines and configurations, such as safety factor q, or triangularity, the convected fraction maybe somewhat higher or lower. No consistent trends in the fraction of pedestal energy convected by an ELM have yet been observed. The variation in convected energy is illustrated in figure 1(a) and (b) where the higher triangularity configuration exhibits nearly a factor of two higher density loss than at lower triangularity. An additional observation from charge exchange recombination (CER) spectroscopy on DIII-D has shown that the fraction of impurity ions expelled at an ELM is the same fraction for that of the main ions [18].
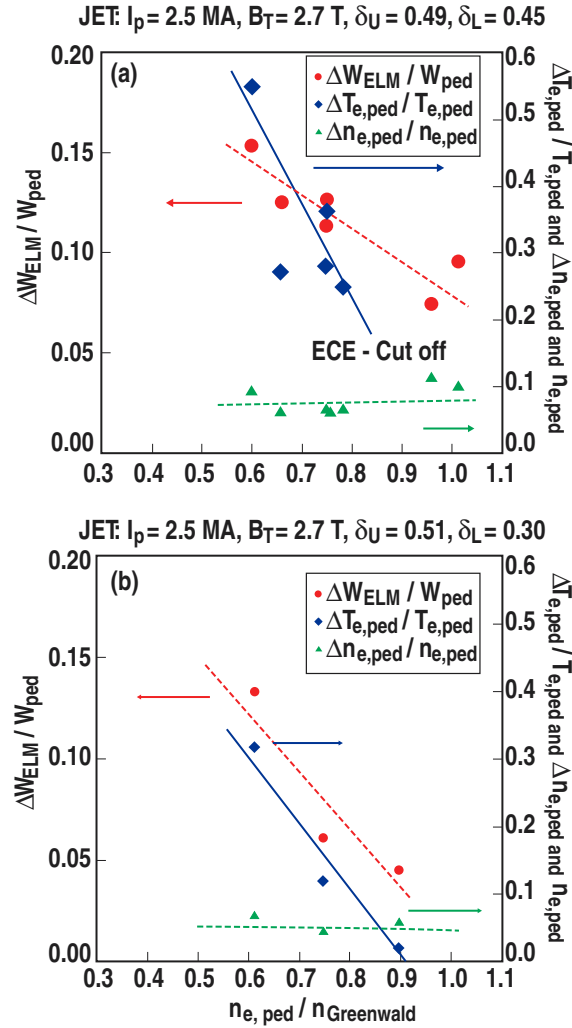
Fig. 1. JET normalized ELM energy loss ($\Delta W_{ELM}/W_{ped}$) and pedestal temperature ($\Delta T_{e,ped}/T_{e,ped}$) and density ($\Delta n_{e,ped}/n_{e,ped}$) drop versus pedestal density normalized to the Greenwald limit ($n_{e,ped}/n_{Greenwald}$) for discharges with (a) high upper and lower triangularities and (b) high upper and medium lower triangularities. At the highest $n_{e,ped}$ the ELM energy loss is due almost entirely to the ELM particle loss. Reference 20 [Reprinted courtesy of AIP, Phys. Plasmas **12**, 2668 (2004).]

In contrast to the density, the ELM perturbation to the electron temperature, or conducted energy, can vary significantly, ranging from greater than 20% at the pedestal top at low density to nearly negligible at high density and collisionality, also shown in figure 1(a) and (b) [16,17]. This variation is not strictly controlled by pedestal collisionality alone, with other factors such as plasma shape and safety factor playing a role. The other component of the conducted energy is the ion temperature. In DIII-D the relative perturbation to T_i is very nearly equal to the T_e perturbation across an ELM and decreases at high density in the same manner [18]. In JT-60U the relative T_i perturbation can be even larger than the perturbation to T_e [19].

The region of plasma affected by an ELM is typically several times the width of the pedestal and has not been observed to vary greatly with density or plasma configuration. The electron and

ion temperature perturbation region is similar in width to the density perturbation. In particular the shape of the temperature perturbation remains nearly constant with only a reduction in magnitude as the ELM energy decreases at high density [20]. The peeling-ballooning eigenmodes driving the ELM perturbation are more localized to the pedestal region and calculated to become narrower at high collisionality where ELMs become smaller [16]. Connecting the linear drive of the mode at onset to the resulting transport is a goal for ELM model development.

The duration and time dependence of the ELM instability can also offer insight into ELM transport processes. The time dependence of several pedestal parameters during a typical ELM in JET is shown in figure 2 [13]. In this example the timing of magnetic fluctuations coincides with a drop in the pedestal electron temperature and rising divertor ion flux. Across a number of devices, configurations and operational regimes, the duration of the ELM instability, and its resulting transport, has been reported within a narrow range of $\sim$200 μs [6,13,16]. A detailed study of ELM duration versus parameters such as toroidal field, or input power to increase the pedestal temperature, could indicate which processes, such as ideal magnetohydrodynamic (MHD) or magnetic reconnection, are most relevant.
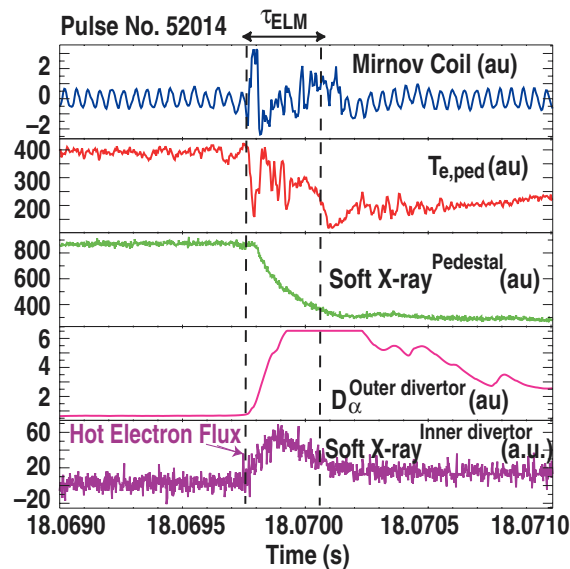
Fig. 2. JET measurements with high time resolution of the MHD activity, pedestal temperature, and soft x-ray emission collapse, and outer divertor D_α emission and inner divertor x-ray bremsstrahlung from hot electron impact during a Type I ELM. The collapse of $T_{e,ped}$, pedestal soft x-ray emission and inner divertor bremsstrahlung emission occur over a time interval of 200-300 ms similar to the period of large MHD activity. Reference 13 [Reprinted courtesy of IOP, Plasma Phys. Control. Fusion **45**, 1549 (2003).]

A number of diagnostics have observed loss of plasma due to an ELM to be localized to the outboard midplane [20-24]. The resulting perturbation to the pedestal density profile has been followed across an ELM by microwave reflectometry and interferometry [23-25]. The pedestal

density at the outboard midplane drops first, flattening the steep gradient within a few hundred µs. The inboard pedestal density collapse follows, delayed by the time for ion sound speed parallel flow from the inboard to the outboard pedestal. These observations are consistent with plasma density rapidly ejected from outboard pedestal by an ELM, followed by parallel convection from inboard to outboard to equalize the density on the closed flux surfaces of the pedestal.

The pedestal electron temperature perturbation occurs over a duration similar to that of the density. In figure 2 the pedestal T_e, as observed by ECE and soft x-ray (SXR) emission, drops during the magnetic fluctuation phase of the ELM, ~200 µs. This is roughly the same time for the pedestal density loss. One should note that the more local ECE measurement exhibits greater fluctuations than the line integrated SXR signal. The duration of the pedestal ion temperature perturbation, however, can be significantly longer. This is illustrated in figure 3 where the ion temporal response to an ELM has been measured in DIII-D with a fast CER diagnostic [18]. In this case the pedestal carbon impurity density drops in a few hundred µs during the rising phase of D_α emission. The inflection point for flattening of the density gradient is just inside the separatrix, similar to reflectometry measurements. The ion temperature gradient immediately decreases slightly, but the overall ion temperature profile does not drop significantly. After the density drop is complete the ion temperature then decays during a time of up to one millisecond. These different time sequences would seem to indicate different mechanisms for the ELM density and temperature transport.
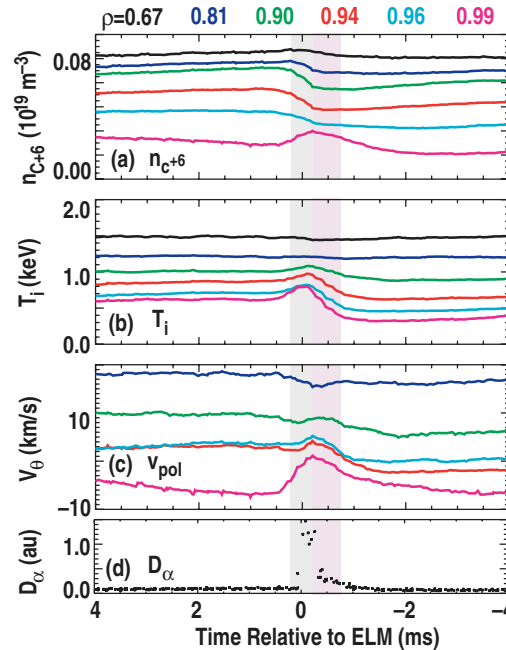
Fig. 3. In DIII-D temporal evolution of (a) n_{c+6}, (b) T_i, (c) V_θ, and (d) midplane D_α for several CER channels sampling the edge plasma during an ELM cycle. The channel locations are $\rho = 0.67$, 0.81, 0.90, 0.94, 0.96 and 0.99. Reference 18 [Reprinted courtesy of AIP, Phys. Plasmas **12**, 056120 (2005).]

The pedestal radial electric field, E_r, is another important characteristic that can be extracted from the CER measurements. Shear, or a well, in the edge E_r is thought to be responsible for stabilizing edge turbulence, resulting in a transport barrier and steep gradients characteristic of the H-mode pedestal. An important component of this parameter, the poloidal velocity, V_θ, is also shown in figure 3. The edge gradients of V_θ quickly flatten within a few hundred μs during the initial phase of the ELM, similar to the density profile. The V_θ gradient then rebuilds in about a millisecond, similar to the ion temperature drop. The E_r well, reconstructed from poloidal and toroidal velocity and the ion pressure gradient, displays a similar time dependence, a rapid collapse followed by a slow rebuilding. The radial profiles of E_r just before an ELM and after its onset are shown in figure 4(a). The deep E_r well quickly collapses to a shallow level and then slowly evolves and deepens until the next ELM.
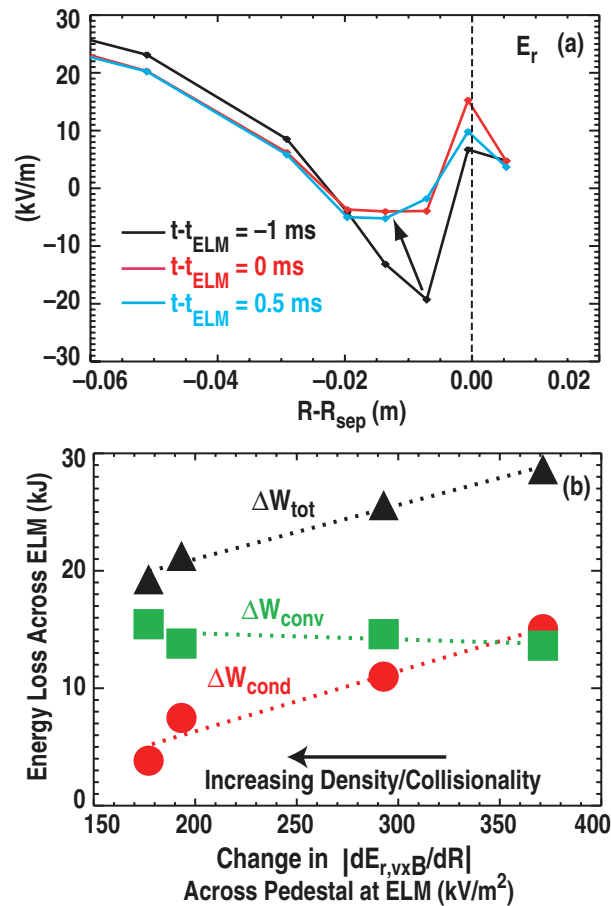
Fig. 4. (a) Radial profile of E_r measured just before and after an ELM crash. (b) Variation of conductive (closed circles), convective (open squares), and total (closed triangles) energy losses induced by the ELM versus the change in the average E_r gradient. The energy loss is the summation of the electron, ion, and impurity energy losses. Reference 18 [Reprinted courtesy of AIP, Phys. Plasmas **12**, 056120 (2005).]

   The magnitude of E_r collapse is correlated with the level of conducted energy in DIII-D, as shown in figure 4(b) [18]. At low density the E_r well is deep with steep temperature gradients in the pedestal. At an ELM the E_r well collapses to the level shown in figure 4(a), while the temperature profile is significantly perturbed resulting in a large conducted energy. At high density the E_r well before an ELM is much shallower, but collapses to the same level as the low density case. At the same time the ELM at high density produces a very small perturbation to the temperature profiles resulting in a negligible conductive component to the ELM energy. This trend, shown in figure 4(b), suggests that the conductive ELM component results from rapid radial turbulent transport when the steep edge temperature gradients are no longer stabilized by a deep E_r well. This possible transport mechanism will be discussed further in Section IV.

III. SOL ELM TRANSPORT

Fast measurements in the SOL and divertor also offer the opportunity to observe ELM evolution and resulting transport. A example of the insight SOL measurements can offer is shown in figure 5, where a visible image of the MAST spherical tokamak (ST) has been taken with a 20 µs exposure time [26]. Extended filamentary perturbations to the outboard edge of MAST plasmas can be observed with a toroidal mode number of approximately 10. Edge filamentary structures have also been observed in the edge plasmas of DIII-D in CIII emission [27]. The toroidal mode number of the visible structures in DIII-D was in the range of n = 15-20, agreeing with the linearly stability analysis indicating the most unstable eigenmodes having the same toroidal mode number. The images from MAST and DIII-D also have characteristics similar to a nonlinear ballooning theory [10,11] that will be discussed further in Section IV.
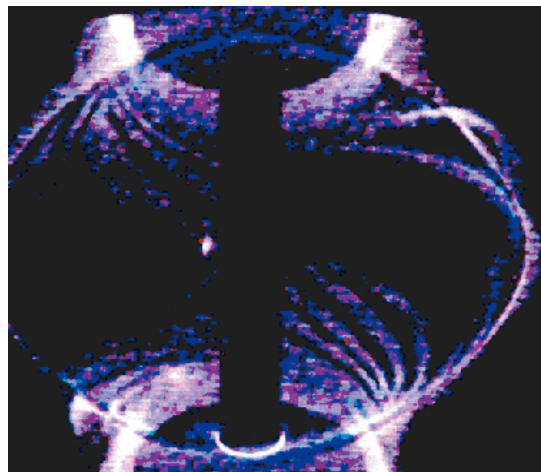
Fig. 5. High-speed video image of the MAST plasma obtained at the start of an ELM. Reference 26 [Reprinted courtesy of IOP, Plasma Phys. Control. Fusion **45**, 1571 (2003).]

Other diagnostics also observe these filaments propagating radially in the SOL. From within the pedestal the filaments have been seen with beam emission spectroscopy (BES) in DIII-D and Thomson scattering in ASDEX-Upgrade to originate as perturbations to the local density inside the separatrix with a spatial scale of less than 2-3 cm [28,29]. Out into the SOL localized views of the outer midplane in visible and infrared (IR) emission have observed interaction of these filaments with material limiters in ASDEX-Upgrade [30,31]. The spatial scale of the filaments in the SOL is typically a few centimeters. Helical stripes in IR camera images of the ASDEX-Upgrade outboard divertor, shown in figure 6, have been interpreted to also indicate the presence of filaments of several centimeters in cross section and intermediate toroidal mode number, 8-12, propagating radially into the SOL [32]. The IR data also indicate the multiple

filaments do not emerge simultaneously, but over a period of roughly 100-200 µs [33]. The filaments have also been occasionally captured in the SOL by Thomson scattering with a measurement on a very short timescale, <1 µs [26,29]. The plasma filaments appear as a bump, or local maximum in the Thomson SOL profile of density and/or temperature.
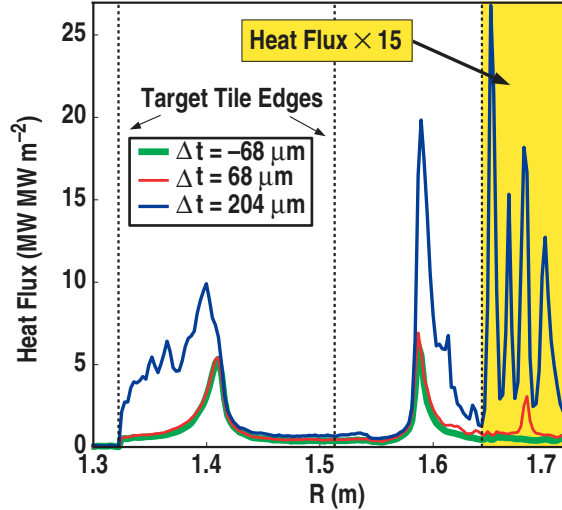
Fig. 6. Divertor heat flux profiles in ASDEX-Upgrade shortly before an ELM, just after ELM onset and at peak ELM heat flux. The shaded region indicates remote tiles with increased heat flux sensitivity. Reference 32 [Reprinted courtesy of IOP, Plasma Phys. Control. Fusion **47**, 815 (2005).]

More detailed measurements of the ELM filament parameters and evolution have been made by Langmuir probes that have been inserted into the edge plasmas of a number of tokamaks, including JET, DIII-D, JT-60U, MAST and ASDEX-Upgrade [28,34-37]. The probes have multiple tips to allow simultaneous measurement of I_{sat}, n_e, T_e and plasma potential, Φ, within the ELM filaments. The signal from a probe in the SOL during an ELM exhibits the typical characteristics shown in figure 7. Shortly after the ELM onset a series of peaks in I_{sat}, with an elevated level in I_{sat} between the peaks, propagate past the probe in the SOL. The envelope of the I_{sat} signal follows the general trend of the midplane D_α, with a duration of about 1-2 ms. The longer duration of the probe signals compared to the 100-200 µs of pedestal fluctuations has yet to be resolved, but may represent the relaxation time of the SOL to the initial ELM particle flux. The initial multiple peaks observed with probes have been interpreted as the result of rotation of the filaments. On ASDEX-Upgrade and MAST, the period between I_{sat} peaks and a measured toroidal rotation characteristic of the plasma just inside the separatrix was used to estimate the toroidal mode number for the ELM filaments at roughly 10, again consistent with linear stability theory [31]. In contrast to the toroidal rotation interpretation, the finite toroidal extent of the IR signatures in ASDEX-Upgrade indicate a much lower toroidal velocity [33]. Also CER and SOL probe measurements from DIII-D and JET indicate that toroidal velocity is carried from the pedestal into the SOL where it is quickly damped a short distance from the

separatrix [28,36]. Reconciling these observations will require measurements of both the toroidal and poloidal velocities of the filaments as they propagate through the SOL.
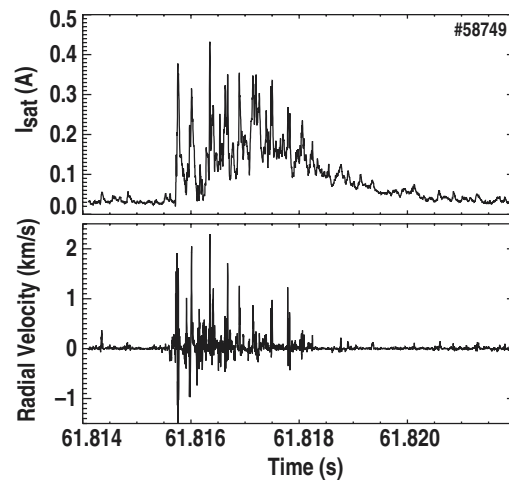
Fig. 7. Time evolution of I_{sat} and the effective radial velocity in the SOL during an ELM in JET. Reference 34 [Reprinted courtesy of Elsevier, J. Nucl. Mater. **337-339**, 722 (2005).]

The ELM filament radial velocity can be determined by measuring the delay from ELM onset until arrival at a probe at different radial locations in the SOL. On MAST this technique indicated that the filaments accelerate from low radial velocity near the separatrix to near 1 km/s 15 cm into the SOL [31]. Similar data analysis on ASDEX-Upgrade reveals a somewhat lower radial velocity and acceleration [31], while JET [38] and JT-60U [37] data, also using the time delay technique, indicate a constant radial velocity in the range of 0.5-2 km/s. An alternative analysis uses the plasma potential from two poloidally separated probe tips to estimate the radial velocity. Using the $E \times B$ analysis, the ELM filament radial velocity in JET and DIII-D has been measured to peak near the separatrix at a level approaching 1 km/s, but with the expansion slowing as the filaments approach the vessel wall [28,34]. A similar radial velocity is confirmed with reflectometry in DIII-D [39]. Understanding these differences is important because the profile of radial velocity could indicate when the filaments detach from the pedestal plasma and connect to the target.

A radial profile of the ELM filament's plasma parameters can be obtained by compiling data from several distinct ELMs as they propagate past a probe at different radial locations. This analysis has produced ELM profiles in DIII-D [28] at high and low density as shown in figure 8. The ELM filament electron temperature is nearly that of the pedestal when it exits the main plasma near the separatrix. However the temperature falls quickly as the filament propagates radially with a fall off length of 1-2 cm at the midplane for both low and high density. The electron density, also shown in figure 8, falls off much more slowly with a ~3 cm characteristic length at high density and 10 cm or more at low density. While the ion temperature is more difficult to measure on the ELM timescale, an estimate of the ELM filament T_i in the far SOL has been made with a retarding field analyzer (RFA) in JET [40]. The RFA measured an ELM

ion temperature of 100-150 eV at the outboard limiter radius for a plasma with a 400 eV pedestal ion temperature. In similar discharges a Langmuir probe measured T_e at ~30 eV in the same location. The rapid decay of T_e and slower decay of T_i and n_e is consistent with parallel losses from the filaments to the divertor targets [41]. This issue will be discussed in more detail in Section IV.
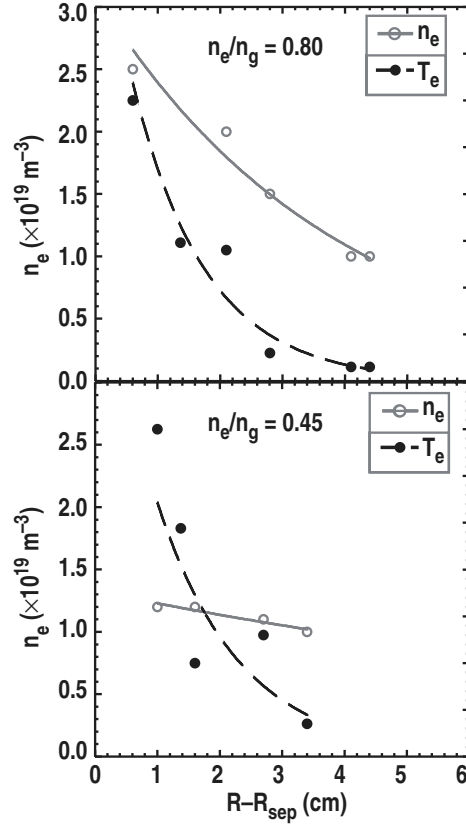
Fig. 8. Radial variation of the ELM peak density and temperature values obtained from probes for (a) high density and (b) low density discharges in DIII-D. The temperature decays quickly with radius in both cases, but the density decay length is much longer at low density. Reference 28 [Reprinted courtesy of APS, Phys. Rev. Lett. **92**, 245002 (2004).]

The ELM filaments described above likely carry a small fraction of the energy and particles lost at an ELM. The filaments propagating radially represent energy convected from the pedestal and would not directly cause a reduction in pedestal temperature. For the convected energy a few estimates of the total particles carried by the propagating ELM filaments also indicate they carry significantly less than half of the total lost particles [31,34]. A typical Type I ELM releases ~10% of the pedestal density times the plasma volume, roughly equivalent to the pedestal density times the pedestal layer volume. While the filaments carry a density approximately that of the pedestal, the volume is significantly less than that of the pedestal layer. While the filaments may not directly carry the majority of the ELM energy or particles, their characteristics still have implications for ELM transport. These issues are discussed in the next section.

IV. IMPLICATIONS FOR ELM TRANSPORT

Recent theoretical and modeling developments of the nonlinear evolution of the Type I ELM instability are consistent with many experimental observations. A nonlinear theory of the ballooning instability predicts the explosive growth of localized filaments extending along magnetic field lines which narrow and twist as they are accelerated out of the pedestal into the SOL [10], similar to many SOL observations noted above. A nonlinear 3D electromagnetic simulation of intermediate wavelength peeling-ballooning modes with the BOUT code also exhibited many of these same features with a number of extended filaments propagating rapidly from the closed flux region into the SOL [11]. One issue to address in the early ELM phase is how the observed slowly growing, or saturated, precursors are triggered into the explosive growth phase.

While the predicted ELM filaments appear to be well confirmed by experiment, their direct convection of plasma into the SOL is inadequate to explain observed ELM losses. To address the additional transport several mechanisms have been proposed to explain how the nonlinear ELM phase leads to the observed ELM energy and particle losses and their dependencies upon pedestal parameters. The first proposed mechanism postulates the filaments remain connected to the hot core plasma, acting as a conduit for fast parallel transport from the pedestal into the SOL. Fast diffusion or instabilities would transfer heat and particles from the extended filaments onto field lines in the SOL and then through parallel transport to the divertor [10]. A second conjecture postulates that the nonlinear phase of filaments and turbulence leads to a tearing and/or ergodization of magnetic field lines within the pedestal. This creates a path for parallel transport from the pedestal directly to the divertor [42,43]. In a third proposed mechanism the propagation of the filament causes a collapse of the H-mode transport barrier by suppressing the edge $E \times B$ flow shear [11]. Strong turbulent transport, driven by the steep edge gradients that are no longer suppressed by the E_r well, results in a rapid loss of particles and energy from the pedestal. While it is possible, or even likely, that all of these mechanisms, and perhaps others, are involved in an ELM it is worthwhile to examine them separately to assess the extent of their contribution to ELM losses. The filaments acting as a conduit for transport from the pedestal to significantly past the separatrix into the SOL, does not seem to be well supported by the observations. The steep fall in electron temperature as the filaments propagate radially is consistent with observations of the bulk of ELM energy deposited in the divertor near the strikepoints. This suggests the filaments no longer have a parallel path to the pedestal plasma within a couple of centimeters outside the separatrix. Also, the low filament T_e would indicate that radial transport from the filament to the SOL to be faster than parallel transport from the pedestal. While rapid radial transport out of a filament may be possible due to MHD instability, this consideration results in essentially a parallel path directly from the pedestal to the target, a

mechanism considered in the next paragraph. In addition the data from Langmuir probes present no evidence of hot pedestal electrons in the filaments after a short distance from the separatrix. Finally the filaments' characteristics have been successfully modeled by treating the filament as a SOL "plasmoid" extending along the magnetic field, with a parallel path to the divertor [41]. In this model the poloidal pressure gradient across the filament coupled with a sheath condition at the target produces an $E \times B$ radial propagation of the filament. The parallel losses in this model have reproduced the rapid decay in T_e and the slower decay of T_i and n_e in the filaments. A fruitful area for future work would be to examine the consistency of the measured filament radial profiles of velocity temperature and density within the framework of this model.

The second mechanism for ELM transport considered here postulates the ELM instability opens a parallel path from the pedestal to the divertor target. This could occur as the ejected filaments are torn from the pedestal plasma, or breakup quickly outside the separatrix, leaving pedestal field lines open to the SOL. Turbulence of the ELM instability itself could also lead to ergodization of the edge. The response of pedestal transport to a parallel loss path has been examined in several studies [13,42]. In this scenario transport from the pedestal is essentially set by ion parallel convection. Hot electrons first stream from the pedestal to the target setting up a sheath that limits heat loss due to a finite ion flux at the target. Electron energy loss from the pedestal is suppressed until ion flux flowing at the sound speed arrives at the target to increase the particle and energy flux through the sheath. The total ELM energy loss is then dependent upon the ratio of the ion parallel transit time to the ELM duration. The sheath is critical if parallel transport from the pedestal is significant because electron thermal conduction would otherwise dominate ELM losses. Kinetic modeling of this process [44] has reproduced several experimental observations, including the duration of the target heat flux scaling with the ion transit time [45]. While a high energy sheath is clearly indicated to play a role in setting the ELM target heat flux spatial profile and temporal evolution, it is not yet established whether the target sheath is a limiting factor in thermal loss from the pedestal during an ELM. Fast simultaneous measurements of T_e in the divertor and midplane could add insight into the role of parallel conduction and the target sheath in ELM transport.

The final mechanism for ELM transport considered here is collapse of the H-mode transport barrier. As summarized above from DIII-D observations, an ELM at low density is shown to reduce the E_r well, concurrent with reductions in the steep gradients of T_e, T_i and n_e. At high density the E_r well reduction is less and the resulting perturbations to T_e and T_i become negligible, though the fractional density loss remains nearly constant. While this is suggestive of a mechanism for the conducted energy loss, there is work required on several fronts to establish the relevance of this process. First, the issue of causality should be addressed. Fast profile measurements could determine if the E_r well collapse precedes the temperature drop, or if the E_r well collapse results from the loss of pedestal pressure. Further work is also needed to characterize the fraction of the density loss carried by the filaments, as opposed to turbulent transport at the ELM, in order to understand how the fractional density loss remains constant while temperature loss is reduced at high density. More fundamentally the relationship between

gradients in T_e, T_i and n_e, and the gradient of E_r in the pedestal needs further experimental and theoretical development. While this is also a goal for prediction of pedestal characteristics it may also aid in understanding the depth of the ELM crash as a response to a flattening of E_r. Finally an estimate of turbulent transport levels for steep gradients is needed. For edge temperature gradients that are far above the critical level for driving strong turbulence in the absence of sheared flow a theoretical estimate of the resulting transport could help determine if turbulent transport due to a flattening of the E_r well could account for a significant fraction of the observed thermal loss within the duration of the ELM.

While the characterization of ELM dynamics, as summarized above, is not complete, a large body of experimental observations has been made. Hopefully these observations, and further results, can serve as an aid and guide in the development of ELM theoretical models and simulations.

REFERENCES

[1]   G. Federici, A. Loarte and G. Strohmayer, Plasma Phys. Control. Fusion **45**, 1523 (2003).

[2]   P.B. Snyder, H.R. Wilson, T.H. Osborne, A.W. Leonard, Plasma Phys. Control. Fusion **46**, A131 (2004).

[3]   W. Suttrop, K. Büchl, H.J. de Blank, et al., Plasma Phys. Control. Fusion **38**, 1407 (1996).

[4]   T. Kass, S. Günther, M. Maraschek, et al., Nucl. Fusion **38**, 111 (1998).

[5]   T. Bolzonella, H. Zohm, M. Maraschek, et al., Plasma Phys. Control. Fusion **46**, A143 (2004).

[6]   N. Oyama, N. Asakura, A.V. Chankin, et al., Nucl. Fusion **44**, 582 (2004).

[7]   E.J. Strait, T.A. Casper, M.S. Chu, et al., Phys Plasmas **4**, 1783 (1997).).

[8]   T.H. Osborne, A.W. Leonard, M.A. Mahdavi, et al., Phys. Plasmas **8**, 2017 (2001

[9]   C.P. Perez, H.R. Koslowski, G.T.A. Huysmans, et al., Nucl. Fusion **44**, 609 (2004).

[10]   H.R. Wilson and S.C. Cowley, Phys. Rev. Lett. **92**, 175006 (2004).

[11]   P.B. Snyder, H.R. Wilson, X.Q. Xu, Phys. Plasmas **12**, 056115 (2005).

[12]   A.W. Leonard, A. Herrmann, K. Itami, et al., J. Nucl. Mater. **266-269**, 109 (1999).

[13]   A. Loarte, G. Saibene, R. Sartori, et al., Plasma Phys. Control. Fusion **45**, 1549 (2003).

[14]   K. Kamiya, et al., submitted this conference

[15]   H. Urano, W. Suttrop, L.D. Horton, et al., Plasma Phys. Control. Fusion **45**, 1571 (2003).

[16]   A.W. Leonard, T.H. Osborne, M.E. Fenstermacher, et al., Phys. Plasmas **10**, 1765 (2003).

[17]   A. Loarte, M. Beoulet, G. Saibene, et al., Plasma Phys. Control. Fusion **44**, 1815 (2002).

[18]   M.R. Wade, K.H. Burrell, J.T. Hogan, et al., Phys. Plasmas **12**, 056120 (2005).

[19]   M. Yoshida, et al., submitted this conference.

[20]   A. Loarte, G. Saibene, R. Sartori, et al., Phys. Plasmas **12**, 2668 (2004).

[21]   T.W. Petrie, J.G. Watkins, L.L. Lao, et al., Nucl. Fusion **43,** 910 (2003)

[22]   M.E. Fenstermacher, A.W. Leonard, P.B. Snyder, et al., Plasma Phys. Control. Fusion **45**, 1597 (2003).

[23]   I. Nunes, G.D. Conway, A. Loarte, et al., Nucl. Fusion **44**, 883 (2004).

[24]   N. Oyama, Y. Miura, A.V. Chankin, et al., Nucl. Fusion **43**, 1250 (2003).

[25]   L. Zeng, G. Wang, E.J. Doyle, et al., Plasma Phys. Control. Fusion **46**, A121 (2004).

[26]   A. Kirk, H.R. Wilson, G.F. Counsell, et al., Phys. Rev. Lett. **92**, 245002 (2004).

[27]   M.E. Fenstermacher, T.H. Osborne, A.W. Leonard, et al., "Structure, Stability and ELM Dynamics of the H-mode Pedestal in DIII-D," General Atomics Report GA-A24937 (2004) and accepted for publication in Nucl. Fusion.

[28]   J.A. Boedo, D.L. Rudakov, E.M. Hollmann, et al., Phys. Plasmas **12**, 072516 (2005).

[29]   B. Kurzan, H.D. Murmann, J. Neuhauser, et al., "Fine Structure of Type-I Edge-Localized Modes in the Steep Gradient Region," accepted for publication in Phys. Rev. Lett. (2005).

[30] A. Herrmann, et al., J. Nucl. Mater. **337-339**, 697 (2005).

[31] A. Kirk, T. Eich, A. Herrmann, et al., Plasma Phys. Control. Fusion **47**, 995 (2005).

[32] T. Eich, et al., Phys. Rev. Lett. **91**, 195003 (2003).

[33] T. Eich, A. Herrmann, J. Neuhauser, et al., Plasma Phys. Control. Fusion **47**, 815 (2005).

[34] C. Silva, B. Goncalves, C. Hidalgo, et al., J. Nucl. Mater. **337-339**, 722 (2005).

[35] B. Goncalves, C. Hidalgo, M.A. Pedrosa, et al., Plasma Phys. Control. Fusion **45**, 1627 (2003).

[36] M. Endler, I. Garcia-Cortes, C. Hidalgo, et al., Plasma Phys. Control. Fusion **47**, 219 (2005).

[37] N. Asakura, M. Takechi, G. Matshunaga, et al., "ELM Propagation and Fluctuations in SOL and Divertor on JT-60U Tokamak," Proceedings of 32nd European Physics Society Conference on Plasma Physics, Tarragona, Spain (2005) Paper P5-006.

[38] W. Fundamenski, W. Sailer, Plasma Phys. Control. Fusion **46**, 233 (2004).

[39] L. Zeng, G. Wang. E.J. Doyle, et al., J. Nucl. Mater. **337-339**, 742 (2005).

[40] R.A. Pitts, W. Fundamenski, et al., "Far SOL ELM Ion Energies in JET," submitted to Nucl. Fusion (2005).

[41] W. Fundamenski, R.A. Pitts, "A Parallel Transport Model of Tokamak Power Exhaust Transients," submitted to Plasma Phys. Control. Fusion (2005).

[42] G. Janeschitz, ITER JCT and Hts, J. Nucl. Mater. **290-293**, 1 (2001).

[43] E.R. Solano, S. Jachmich, F. Villone, et al., J. Nucl. Mater. **337-339**, 747 (2005).

[44] A. Bergmann, Nucl. Fusion **42**, 1162 (2002).

[45] T. Eich, A. Herrmann, P. Andrew, et al., J. Nucl. Mater. **313-316**, 919 (2003).

ACKNOWLEDGMENT